

RSC Advances



This is an *Accepted Manuscript*, which has been through the Royal Society of Chemistry peer review process and has been accepted for publication.

Accepted Manuscripts are published online shortly after acceptance, before technical editing, formatting and proof reading. Using this free service, authors can make their results available to the community, in citable form, before we publish the edited article. This *Accepted Manuscript* will be replaced by the edited, formatted and paginated article as soon as this is available.

You can find more information about *Accepted Manuscripts* in the [Information for Authors](#).

Please note that technical editing may introduce minor changes to the text and/or graphics, which may alter content. The journal's standard [Terms & Conditions](#) and the [Ethical guidelines](#) still apply. In no event shall the Royal Society of Chemistry be held responsible for any errors or omissions in this *Accepted Manuscript* or any consequences arising from the use of any information it contains.

Electrical characterization of amorphous LiAlO₂ thin films deposited by atomic layer deposition

Yang Hu^{a,*}, Amund Ruud^a, Ville Miikkulainen^b, Truls Norby^a, Ola Nilsen^a, Helmer Fjellvåg^a

^aCentre for Materials Science and Nanotechnology, Department of Chemistry, University of Oslo

P.O. Box 1126, Blindern, NO-0318 Oslo, Norway

^bLaboratory of Inorganic Chemistry, University of Helsinki, P.O. Box 55, FI-00014 Helsinki, Finland

Abstract

LiAlO₂ thin films deposited by atomic layer deposition (ALD) have potential application as electrolyte in three-dimensional (3D) all-solid-state microbatteries and in this work the Li-ion conductivity of such films is investigated by both in-plane and cross-plane methods. LiAlO₂ thin films with a Li composition of $[Li]/([Li] + [Al]) \approx 0.46$ and amorphous structure were grown by ALD with thicknesses of 90, 160 and 235 nm on different substrates. The electrical characterization was carried out by impedance spectroscopy using inert electrodes over a temperature range of 25–200 °C in inert atmosphere. In-plane conductivities were obtained from films on insulating sapphire substrates and cross-plane conductivities were measured from films on conducting titanium substrates. For the first time, comparison of the in-plane and cross-plane conductivities in these ALD LiAlO₂ films has been achieved. More comparable results are obtained by using cross-plane method while in-plane conductivity demonstrates a considerable thickness-dependence with thinner film thickness. The room-temperature conductivity of the LiAlO₂ films has been determined to be in the order of $10^{-10} \text{ Scm}^{-1}$ with an activation energy of *ca.* 0.8 eV.

Key words: Atomic Layer Deposition, ALD; thin films; ionic conductivity, Li-ions, in-plane, cross-plane; LiAlO₂, amorphous

1. Introduction

Future Li-ion battery designs may rely on the utilization of suitable solid-state electrolytes. Their application will circumvent the safety hazards from the release of flammable and poisonous gases during decomposition of liquid electrolytes and open for a larger degree of freedom in the design of the battery structures¹. The major obstacle for the introduction of such solid-state electrolytes is their low ionic conductivity, which can be compensated by the utilization of thinner electrolytes provided that they can be deposited as pinhole-free films²⁻⁴. For conventional two-dimensional (2D) design using thin film electrolytes, a room temperature conductivity above 10^{-6} Scm^{-1} ^{5,6} is required, such as the state-of-the-art lithium phosphorus oxynitride (LiPON) thin film. However, this 2D design suffers from a limited capacity per footprint area (Ah cm^{-2}) and a low power density. The current focus for all-solid-state batteries is therefore on the realization of three-dimensional (3D) microbattery designs, which can appreciably enhance the active electrode area inside the batteries and thus increase the power density^{1,7,8}. A key factor is a thin film process capable of depositing homogeneous and pinhole-free films onto complex structures with large surface areas. Atomic layer deposition (ALD) has proven to be a promising technique for such applications⁹. It is based on self-limiting gas-to-surface reactions that ensure highly conformal growth over complex geometrical shapes¹⁰. Previous works have suggested ALD as a potential and suitable tool to achieve both solid-state and nanostructured design for Li-ion batteries, opening up new possibilities for materials and architectures in 3D all-solid-state batteries¹¹⁻¹³.

The deposition of Li-containing thin films by ALD was first reported in 2009⁹ for the formation of Li_2CO_3 . Since then, ALD has been applied for coating barrier layers onto electrode materials in traditional Li-ion batteries with liquid electrolyte in order to minimize the so-called solid electrolyte interface (SEI) formation as well as for the deposition of active battery electrode materials¹⁴⁻¹⁶. The exploitation of thin film solid-state Li-ion electrolytes by ALD is still considered immature and there are very few reports on the Li-ion conductivity of the deposited films. Liu *et al.* obtained a room-temperature conductivity of $2 \times 10^{-8} \text{ Scm}^{-1}$ for a $\text{Li}_{5.1}\text{TaO}_z$ ALD thin film¹². Aaltonen *et al.* deposited $\text{Li}_2\text{O}-\text{Al}_2\text{O}_3$ thin films, targeted as a

barrier layer between the Li anode and the lithium lanthanum titanate $[(\text{Li}, \text{La})_x\text{Ti}_y\text{O}_z, \text{LLT}]$ electrolyte¹¹, and they obtained an ionic conductivity of $1 \times 10^{-7} \text{ Scm}^{-1}$ at 300 °C for the film subjected to a post-annealing process at 700 °C for 5 h, which may however have induced crystallization in the as-deposited amorphous structure. Recently, Park *et al.*¹⁷ investigated LiAlO_2 ALD films with a thickness of 50 nm grown onto quartz substrates, and obtained a promising room-temperature conductivity of $5.6 \times 10^{-8} \text{ Scm}^{-1}$ in ambient air. Very recently, Kozen *et al.* deposited LiPON by ALD and obtained a conductivity of $1.45 \times 10^{-7} - 3 \times 10^{-7} \text{ Scm}^{-1}$ with increasing N content (1.8 % – 16.3%)¹⁸. However, this conductivity was extracted from the impedance measured in a LiPON/organic liquid electrolyte/Li metal coin cell using LiPON as working electrode, and it is not unambiguous to assign the result to the bulk conductivity of the electrolyte. It is worth noting that in some of the aforementioned works, the conductivity of Li-containing thin films are measured at higher temperature (> 100 °C). This may be due to high measured resistances beyond instrument capability, arising from low ionic conductivity and the commonly used in-plane geometry.

Characterization of electrical conductivity of thin films or membranes can be performed through two different geometrical configurations as demonstrated in **Fig. 1**. One comprises cross-plane conductivity of films deposited either directly onto a conducting substrate (e.g. stainless steel, Ti), or onto a conducting interlayer (e.g. platinum) coated on an insulating support substrate (e.g. sapphire, Al_2O_3)^{19,20}. The conducting substrate or the interlayer serves as bottom electrode, and the top electrode is deposited on the surface of the film. The cross-plane conductivity configuration has been widely applied for the characterization of solid-state electrolytes of Li-ion batteries, however mostly reported on bulk films with thicknesses in the micron range^{19,21}. For thin films, the application of this geometry is limited by short-circuits due to inherent pinholes, micro-cracks, structural change, and thermal effects at elevated temperatures as well as damages caused by experimental handling. An alternative configuration is the in-plane geometry^{22,23}, where films are deposited onto an insulating substrate, with 2 or 4 co-planar electrodes on the film surface. This configuration gives rise to a wider choice of substrates and circumvents the aforementioned short-circuit issues, but does not reflect the conductivity in the direction intended for electrolyte application and can be

affected by anisotropy caused by texture and other structural effects, such as grain boundaries and interfacial lattice mismatch. Moreover, in-plane measurements on resistive systems may be influenced by parasitic parallel surface, interface, and substrate conductance. From a practical point of view, characterization of conductivity on thin films with a thickness down to the nanometer-scale introduces extra challenges. It is also necessary to carefully control the atmosphere and temperature range if it is the intention to maintain a pristine amorphous state.

The present work aims to investigate the electrical conductivity of LiAlO_2 thin films prepared by ALD, which has been suggested as an alternative electrolyte¹¹ or protection layer²⁴ showing good stability towards currently used electrode materials. Both In-plane and cross-plane measurements were performed on LiAlO_2 thin films deposited onto insulating sapphire and conducting Ti substrates, respectively. Room-temperature conductivity is readily measured, and the temperature-dependent ionic conductivities were obtained up to 200 °C. Results from in-plane and cross-plane methods were compared with three different film thicknesses.

2. Experimental

Thin films of nominal composition LiAlO_2 were prepared by Atomic Layer Deposition (ALD) using a modified process based on the one described previously¹¹. All films were deposited with an ASM F-120 Sat reactor at 225 °C. Trimethyl aluminium (TMA) (Witco GmbH, 98 %) was used as aluminium source and lithium trimethyl silanolate (LiTMSO) (Aldrich, 97%) as lithium source. Ozone (O_3 , concentration $\sim 200 \text{ g/Nm}^3$) generated by an IN USA AC series ozone generator from oxygen (99.6% O_2 , AGA) and water (H_2O , 25 °C) were used as oxygen sources. N_2 (g) was used as pulse and purge gas, generated by a Schmidlin-Sirocco 5 generator (99.999% purity considering $\text{N}_2 + \text{Ar}$). LiAlO_2 was deposited from the pulsing sequence [TMA (0.5 s pulse/3 s purge) + O_3 (3/5) + LiTMSO (5/2) + H_2O (0.5/5)].

The films were deposited onto conducting Ti (ASTM, Astrup AS), insulating sapphire ($\alpha\text{-Al}_2\text{O}_3(0001)$, UniversityWafer) and Si (111) (Coating And Crystal Technology Inc.) substrates. The latter was used as reference sample for thickness, structure and composition analyses. The film thickness was determined by spectroscopic ellipsometry (alpha-SE, J. A. Woollam Co., using the Cauchy function) using films on Si substrates. The structure of as-deposited films and films annealed at 600 °C and 950 °C in air was investigated using Grazing Incidence X-ray Diffraction (GIXRD) analysis on the film on Si (111) substrate. The elemental composition was determined by the time-of-flight elastic recoil detection analysis (TOF-ERDA), yielding an atomic ratio of Li:Al = 1:1.16, denoted as LiAlO_2 in this work with a lithium cation content ratio $[\text{Li}]/([\text{Li}]+[\text{Al}])$ close to 0.46 for the as-deposited films.

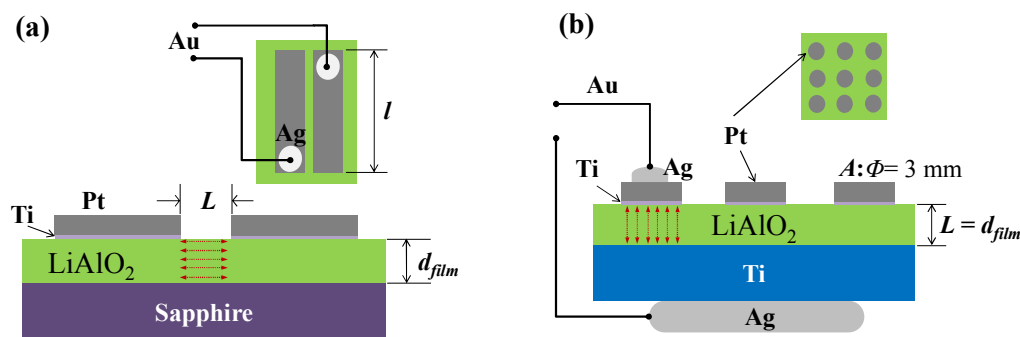


Fig. 1. Sketches of the (a) in-plane and (b) cross-plane geometrical configurations for thin film conductivity measurement. L : distance between the parallel band electrodes, l : length of band electrodes, d_{film} : film thickness, A : electrode area. Red arrows indicate the current pathway.

Electrodes consisting of a 100 nm Pt film on a 5 nm Ti adhesion layer were deposited by e-beam evaporation (Leybold DC V 6-12 kV). The growth rate was 0.2 Å/s for Ti and 0.3-0.5 Å/s for Pt. Parallel band electrodes were made on the surface of LiAlO_2 films on sapphire substrate for in-plane conductivity measurement. Multiple round electrodes with a diameter of 3 mm were applied to the films on Ti substrate for cross-plane conductivity measurements. These Pt electrodes were firstly examined to exclude the area in the film with pinholes. Au wires were attached on top of the Pt electrodes using Ag paste (Aldrich, 735825-25G), dried at 120 °C for 1 h in ambient air, to obtain softer contacts and minimize risks of film damage. The prepared samples were placed in a ProboStat sample holder (NorECs, Norway) for the

conductivity measurements, and an outer steel tube was used to shield the system and contain controlled atmospheres. The configurations of in-plane and cross-plane measurements utilized in this work are illustrated in **Fig. 1**. The Pt electrode/film cross-section of a 90 nm film on Si (111) substrate was cut by Focused Ion Beam (FIB) (FEI Helios NanoLab) and observed by SEM-EDX (HITACHI SU8230 – Bruker Quantax). Scanning electron microscopy (Quanta 200 FEI) was used for the top view of the electrodes after electrical measurement.

The electrical conductivity was measured by two-electrode impedance spectroscopy (Novocontrol Alpha-A + POT/GAL 15V 10A, Novocontrol Technologies) over a frequency range from 1 MHz to 0.05 Hz with an AC amplitude of *50 ca.* 70 mV (50 mVrms). Room-temperature conductivities were measured in ambient air, and the temperature-dependent measurements were performed in dry Ar from room temperature to ~ 200 °C at heating and cooling rates of 2 °C/min. At each temperature, a stabilization period of 30 min was applied prior to data acquisition. The recorded impedance spectra were analyzed in terms of equivalent circuits using *ZView2* software (Scribner Associates Inc.). The conductivity was calculated by the resistance obtained from the data fitting R and the in-plane or cross-plane geometrical considerations, as shown in equations (1) and (2), respectively:

$$\sigma_{in} = \frac{L}{R \times A_{in}} = \frac{L}{R \times (l \times d_{film})} \quad (1)$$

$$\sigma_{cross} = \frac{d_{film}}{R \times A_{cross}} = \frac{d_{film}}{R \times A_{electrode}} \quad (2)$$

3. Results and discussions

The amorphous structure of the LiAlO₂ films investigated in this work is confirmed by GIXRD, as shown in **Fig. 2**. Both as-deposited film and the film annealed at 600 °C exhibit amorphous structures. The transition to crystallinity is observed in the films annealed to 950 °C.

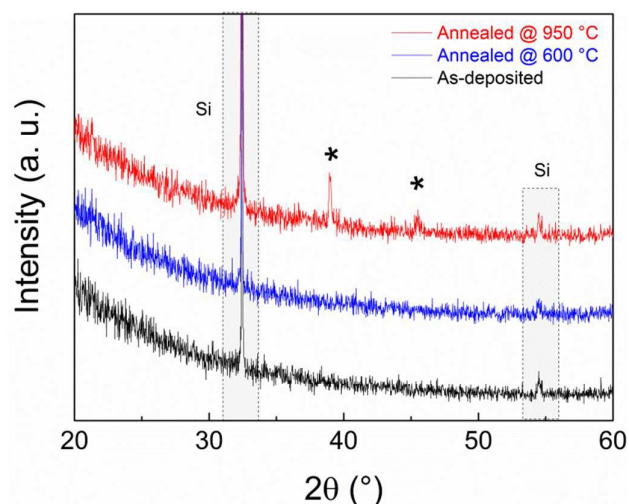


Fig. 2. GIXRD of LiAlO_2 film on Si (111) substrate. * represents the crystalline LiAlO_2 .

FIB-cut 90 nm LiAlO_2 film on Si (111) substrate after Pt deposition exemplifies the cross-sectional morphology of electrode/film interface (**Fig. 3**), displaying good connection between Pt layer and LiAlO_2 film. Top-view SEM images of the electrode contacts shows that the E-beam evaporated Pt electrodes exhibited good adhesion and stability under the experimental conditions of this work (**Fig. 4**). No distinct delamination of Pt layer or agglomeration of Pt grains was observed after the thermal cycles, whatever the substrates. Only minor cracks/fissures were visible close to the Ag/Pt boundary, which is believed to have negligible effect on the measurements.

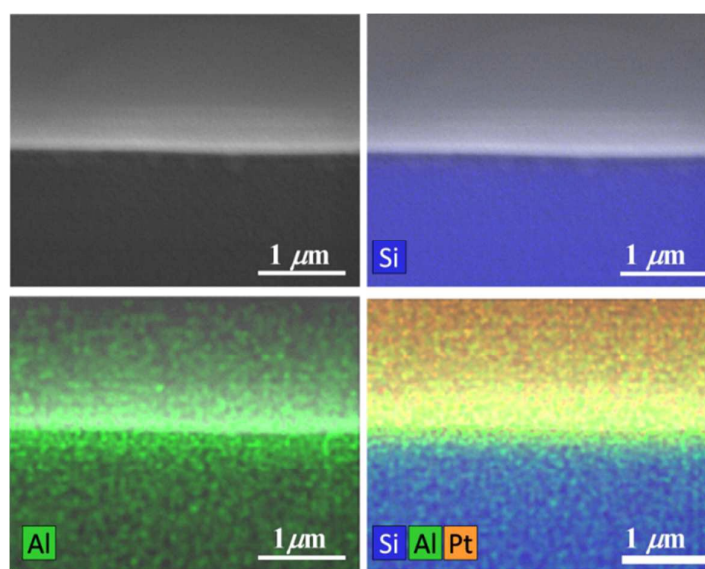


Fig. 3. Cross-sectional SEM-EDX of a reference 90 nm- LiAlO_2 film on Si (111) substrate with Pt

coated on top of the film.

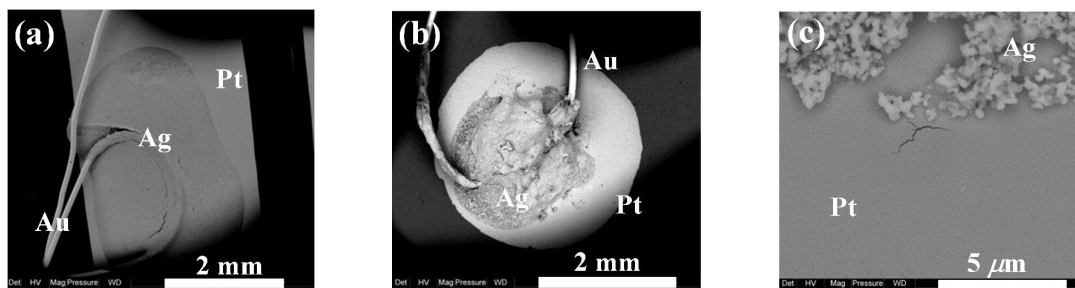


Fig. 4. Top-view SEM images of electrode contacts on top of LiAlO_2 thin films after conductivity measurements: (a) band electrode for film on sapphire substrate; (b) circular electrode for film on Ti substrate; (c) boundary of Ag/Pt.

The electrical conductivity of as-deposited LiAlO_2 films with three thicknesses, 90, 160 and 235 nm was investigated by impedance spectroscopy. **Fig. 5** shows the Nyquist plots of the in-plane impedance of the 160 nm LiAlO_2 film on a sapphire substrate. Typical impedance spectra consist of one semi-circle in the high-frequency region and a low-frequency inclined line. The high-frequency semi-circle can be ascribed to the response of the film bulk, presumably reflecting Li-ion conduction. The low-frequency inclined line represents the impedance of the Li-ion-blocking electrode/electrolyte interface, which is commonly considered as a typical indication of predominantly ionic conduction in the electrolyte²⁵⁻²⁷. The equivalent circuit used to model the impedance spectrum is shown as inset in **Fig. 5**, in which R_b represents the bulk resistance of the film and is used to calculate the conductivity using equation (1). The constant phase element CPE_e takes into account the capacitive contribution of the electrodes associated with the accumulation of charge carrying ions at the electrolyte/electrode interface. Due to the small cross-sectional area of the conductivity pathway – resulting from the small film thickness – the geometrical capacitance of the film bulk becomes very small and is completely masked by the stray capacitance CPE_{stray} from the substrate and setup^{28,29}.

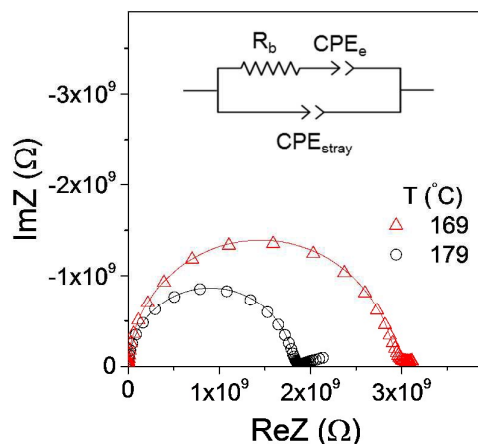


Fig. 5. Impedance spectra of a 160 nm LiAlO₂ thin film on sapphire substrate obtained by in-plane measurement. The equivalent circuit used for data fitting is shown in the inset, and the solid lines of the graphs represent the fitting results.

The in-plane conductivities of 90, 160 and 235 nm LiAlO₂ films obtained from impedance spectra are shown as a function of temperature in **Fig. 6**. The conductivities increase exponentially with increasing temperature, indicating a thermally activated conduction mechanism. However, anomalously high conductance was observed when measured in ambient air or at the beginning of heating in dry Ar, as indicated by the curves in **Fig. 6**. This is attributed to residual water remaining from the ALD cycling or surface adsorbed water from ambient air, giving rise to an additional fast conduction pathway along the surface. When measured in dry atmospheres (here dry Ar), it is permanently eliminated after initial heating. The obtained conductivities otherwise show good reproducibility between increasing and decreasing temperature and can be interpreted and fitted according to an Arrhenius-type behavior for diffusing carriers:

$$\sigma T = \sigma_0 \exp(-E_a / kT) \quad (3)$$

where E_a denotes the activation energy, σ_0 is the pre-exponential factor, k is Boltzmann constant, and T is the absolute temperature. The activation energies and pre-exponential factors obtained from cooling are listed in **Table 1**, along with the room-temperature conductivities. It can be seen that the in-plane conductivity varies pronouncedly with different film thickness.

The thinnest film of 90 nm exhibits the highest conductivity of $\sim 10^{-9} \text{ Scm}^{-1}$ which is one order of magnitude higher than the others. This is in agreement with the abovementioned thickness-dependence in previous reports. However, it is not evident here to draw a simple “thickness to conductivity” relation since the 235 nm films does not exhibit the lowest conductivity.

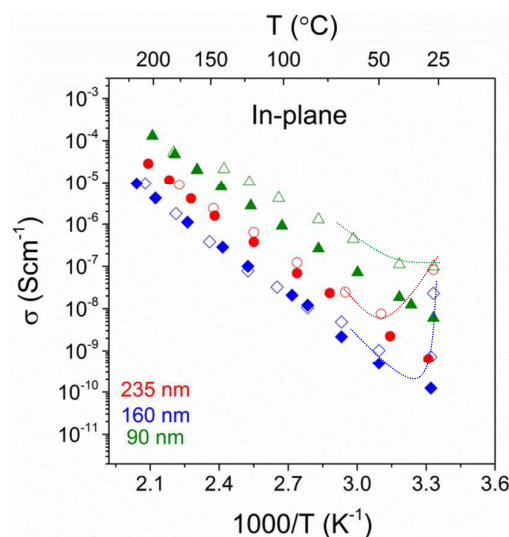


Fig. 6. Conductivities of LiAlO_2 thin films on sapphire substrate obtained by in-plane measurements in dry Ar, from heating (open symbols) and cooling (solid symbols). Curves represent the anomaly during first heating, attributed to adsorbed water.

Fig. 7 shows the cross-plane complex impedance of a 160 nm LiAlO_2 thin film on Ti substrate. In this geometry, both contributions of thin film bulk and the electrodes can be observed at low temperature (**Fig. 7 (a)**). It can be fitted using the equivalent circuit depicted in **Fig. 7 (c)**. A high-frequency semi-circle associated with the contribution of thin film bulk is represented by the bulk resistance R_b in parallel with a capacitive CPE_g mainly representing the geometrical capacitance of the thin film material. The low-frequency linear part of the curve is typical of a blocking electrode (CPE_e), indicating the ionic character of the conduction. It is worth noting that the stray capacitance, which was dominating in the in-plane impedance spectra, is relatively small here in the cross-plane geometry compared to the capacitive contribution of the film bulk, and can thus be neglected. Loss tangent plots help to distinguish between the high- and low-frequency regions, as shown in **Fig. 7 (b)**. The peak value in $\tan\delta$

spectra (indicated by the arrows) separates the electrode process towards lower frequency. It evolves to higher frequency with increasing temperature, as exemplified here from 24 to 61 °C, due to a decrease in the time constants of corresponding bulk and electrode transport processes.

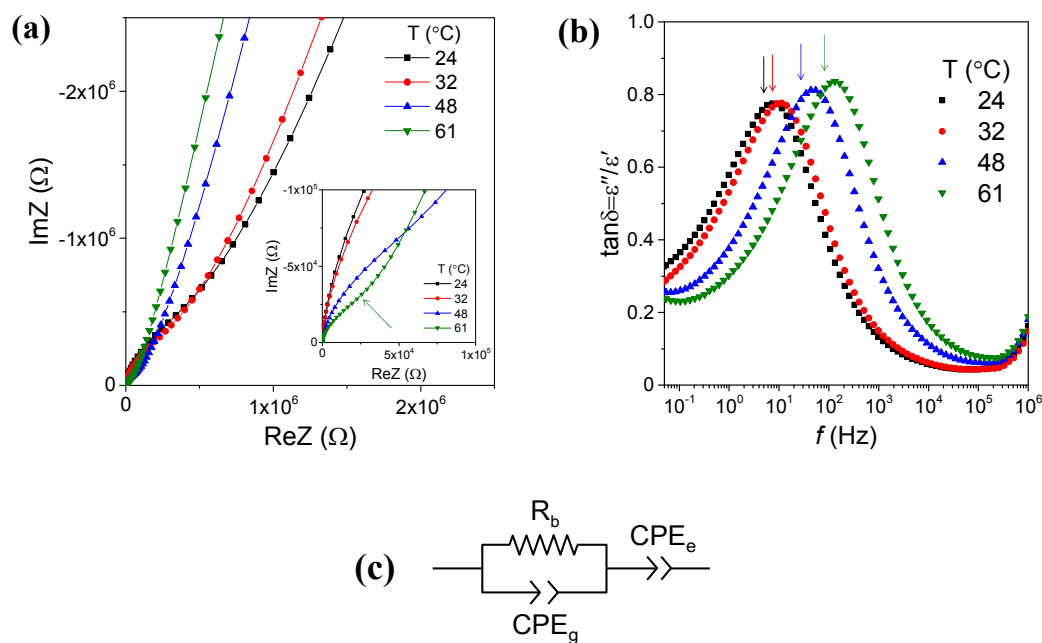


Fig. 7. Impedance spectra of a 160 nm LiAlO₂ film on Ti substrate obtained by cross-plane measurement at low temperatures: (a) Nyquist plots; (b) loss tangent spectra: ϵ' – real and ϵ'' – imaginary part of the complex permittivity; (c) the corresponding equivalent circuit.

The reproducibility of the conductivities obtained with the cross-plane configuration was examined by measuring two electrodes on the same thin film sample at each temperature, as exemplified in **Fig. 8 (a)** for the 160 nm LiAlO₂ film. The good agreement indicates a good uniformity in the film and the deposited electrodes. During the first heating process (**Fig. 8 (a)**, open symbols), there was no remarkable conductivity enhancement at low temperature, and reproducible results were observed over the entire temperature range (RT–200 °C). In comparison to the in-plane measurement, the cross-plane method thus proves to be less sensitive to adsorbed water, which is reasonable since the cross-plane conduction pathway within the film lies between the Ti substrate and Pt electrode, without surface exposed to ambient air. Moreover, the films and electrodes exhibit a good thermal stability over the investigated temperature range **Fig. 8 (b)** shows the Arrhenius plots of conductivity obtained

from 90, 160 and 235 nm LiAlO₂ thin films. A good agreement is evidenced using the cross-plane method without considerable thickness-dependence. Compatible room-temperature conductivity is obtained for 90, 160 and 235 nm LiAlO₂ films, being 2.4×10^{-10} , 2.8×10^{-10} and 2.5×10^{-10} Scm⁻¹, respectively.

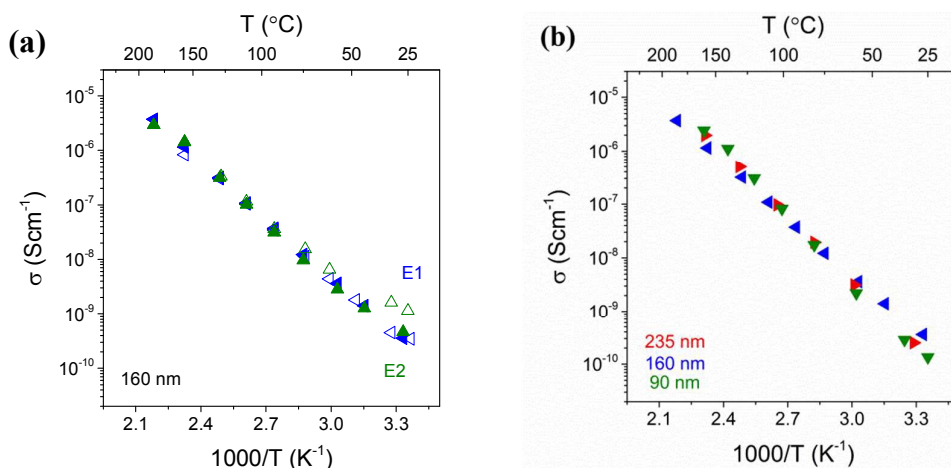


Fig. 8. Conductivities of LiAlO₂ thin films on Ti substrate obtained by cross-plane measurement in dry Ar, (a) from two different electrodes E1 and E2 on the same 160 nm LiAlO₂ thin film during heating (open symbols) and cooling (solid symbols). (b) Comparison of 90, 160 and 235 nm LiAlO₂ films.

A summary of the conductivity in these LiAlO₂ films is presented in **Fig. 9**, with the comparison of thickness and geometry configuration. The room-temperature conductivities, activation energies and the pre-exponential factors obtained from the Arrhenius relation are listed in **Table 1**. The ionic conductivity of materials with a single charge carrier can be expressed in terms of the charge mobility and the concentration of charge carriers, and the diffusion coefficient can be derived by the Nernst-Einstein relationship:

$$\sigma_i = z_i e c_i \mu_i = \frac{(z_i e)^2 c_i}{kT} D_i \Rightarrow D_i = \frac{\sigma_i kT}{(z_i e)^2 c_i} \quad (4)$$

where c_i denotes the concentration of mobile ions of charge $z_i e$ and charge mobility μ_i , and D_i is the random (or self) diffusion coefficient. A hopping mechanism with a correlated jump phenomenon has been proposed also for amorphous materials in relation to the short and long range order effects on the mobility of lithium ions in disordered structure³⁰. In accordance

with the diffusion model, the activation energies reported in **Table 1** reflect fitting of the Arrhenius equation in the form of Eq. (3). In terms of Li ions – which have a concentration in the material independent of temperature – the activation energy of *ca.* 0.8 eV reflect that of the mobility and diffusivity of Li ions. On a more mechanistic level it is still open whether the energy reflects only the barrier for disordered Li ions (or defects) to jump, or also contains formation of disorder (defects) as such.

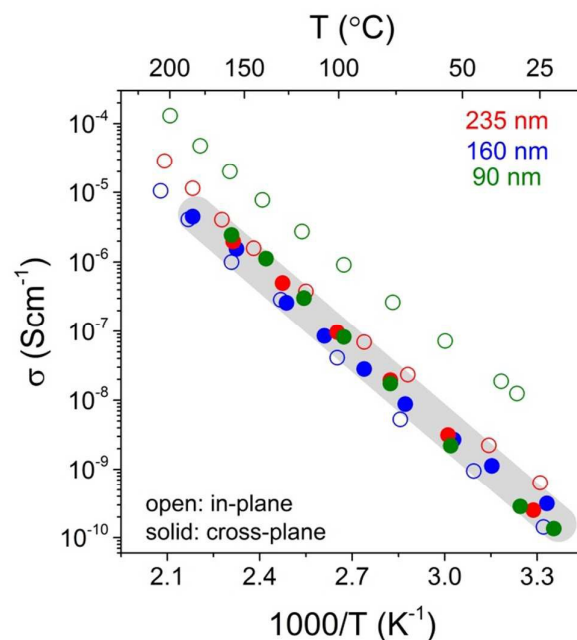


Fig. 9. Conductivities of 90, 160, and 235 nm LiAlO₂ thin films obtained by in-plane (open symbols) and cross-plane (solid symbols) measurements during cooling in dry Ar. Grey area emphasize the cross-plan conductivities.

The variation of in-plane conductivities in the 90, 160 and 235 nm films might be due to the structural modulation or the hetero-interface effect such as film/substrate misfit, which commonly leads to a thickness-dependence in the in-plane conductivity³¹. One may also consider the variation in charge carrier density related to the space charge layer (*SCL*) which will be more pronounced in thin films with thickness comparable to the length of the *SCL* region. For example, Li *et al.* studied the in-plane conductivity of LiPON thin films³² and reported what was interpreted as a transition from ionic conductivity to mixed ionic-electronic conductivity when film thickness was reduced from 50 nm to 40 nm due to the electronic

conduction induced by an enlarged *SCL* region in heterojunctions. Furthermore, a surface enrichment of C or H from the ALD deposition may vary with the number of pulsing cycles, resulting in differences in surface composition and conduction in as-deposited films of different thickness. The in-plane conductivities in our work might be influenced by all the aforementioned factors. One may also notice that for thicker films of 160 and 235 nm, the in-plane and cross-plane conductivities are within the same order of magnitude and a distinct discrepancy is demonstrated in 90 nm films. This leads to a suspect conductivity enhancement from reduced film thickness. Further work with ultra-thin and thicker films would help to clarify this “thickness to conductivity” relation, which is however beyond the scope of this work. Reproducible conductivities are obtained by cross-plane method, and independent of film thickness. This may indicate that in this work the cross-plane method represents better the bulk conductivity of the films, and thus the room temperature conductivity can be drawn to $\sim 10^{-10} \text{ Scm}^{-1}$. Nevertheless, from a practical point of view, the experimental difficulties of measuring 90 nm film has been drastically increased. There was larger probability of short-circuiting from pinholes and the film became more vulnerable to the damages caused by sample handling and thermal effects.

Table 1 Room temperature conductivity and fitting results from the Arrhenius relation

Thickness (nm)	90		160		235	
Geometry	in-plane	cross-plane	in-plane	cross-plane	in-plane	cross-plane
$\sigma_{300K} \text{ (Scm}^{-1}\text{)}$	5.1×10^{-9}	2.4×10^{-10}	1.0×10^{-10}	2.8×10^{-10}	4.3×10^{-10}	2.5×10^{-10}
$\sigma_0 \text{ (Scm}^{-1}\text{K}^{-1}\text{)}$	1.9×10^6	7.4×10^6	1.3×10^6	1.5×10^5	2.1×10^6	6.1×10^6
$E_a \text{ (eV)}$	0.72(1)	0.85(2)	0.82(2)	0.73(1)	0.79(1)	0.84 (2)

Overall, the ALD LiAlO_2 thin films investigated in this work with amorphous structure and a Li cation ratio $[\text{Li}]/([\text{Li}]+[\text{Al}]) \approx 0.46$ exhibit room-temperature conductivities larger than $10^{-10} \text{ Scm}^{-1}$. These are considerably higher than those reported for single-crystalline³³ and polycrystalline $\gamma\text{-LiAlO}_2$ ³⁴ (**Table 2**), probably benefiting from the amorphous nature with isotropic conduction. Compared to crystalline LiAlO_2 , the increased disorder in glassy or amorphous structure gives rise to an increased ionic mobility and suppressed electronic mobility, resulting in predominantly ionic transport characteristics³⁵ as well as enhanced ionic

conductivities. A better agreement has been found in an early report on bulk $\text{Li}_2\text{O}-\text{Al}_2\text{O}_3$ glasses³⁵, in which the extrapolated room-temperature conductivity is $3 \times 10^{-11} \text{ Scm}^{-1}$ for a Li cation ratio $[\text{Li}]/([\text{Li}] + [\text{Al}]) = 0.6$ and $5 \times 10^{-8} \text{ Scm}^{-1}$ for $[\text{Li}]/([\text{Li}] + [\text{Al}]) = 0.7$. Recently, Park *et al.*¹⁷ reported an extrapolated $\sigma_{RT} = 5.6 \times 10^{-8} \text{ S cm}^{-1}$ for an ultrathin (50 nm) ALD LiAlO_2 film, which was obtained by in-plane measurement over 300–400 °C in ambient air. Though the exact Li content is lacking, one can assume based on their previous work on ALD process²⁴ that this enhanced conductivity value may partially result from a high Li cation percentage approaching 0.82, which can only be achieved in relatively thin film. Therefore, it is reasonable to believe that the comparatively low Li cation ratio (0.46) in our work accounts for the lower conductivity, but, on the other hand, allows obtaining thicker films (90, 160 and 235 nm). With respect to the application in solid-state batteries, the conductivities of the ALD LiAlO_2 films reported in this work are still inadequate for a solid-state electrolyte. Further modifications in the ALD processes, for example altering the pulse ratios between the Li and Al cycles in order to increase the Li content, could be considered for improving the conductivity³⁶.

Table 2 Comparison of conductivities of different types of LiAlO_2 (* – extrapolated from high temperature results)

Materials	Experimental conditions	σ_{RT} (S cm^{-1})	E_a (eV)	Ref.
ALD LiAlO_2 thin films, on sapphire and Ti substrates	Impedance, In-plane and cross-plane, 200 °C – RT, dry Ar	$\sim 10^{-10}$	0.7~0.8	This work
ALD LiAlO_2 thin film on quartz substrate	Impedance In-plane, 300–400 °C, ambient air	5.6×10^{-8} *	0.56	17
Single-crystalline γ - LiAlO_2	AC conductivity, 423-623 K	$\sim 1 \times 10^{-17}$ *	1.14(1)	33
Polycrystalline γ - LiAlO_2	AC conductivity 450–1000 °C, dry Ar	2×10^{-14} *	0.81 (extrinsic) 1.3 (intrinsic)	34
Rapidly quenched glasses 0.6 Li_2O -0.4 Al_2O_3 0.7 Li_2O -0.3 Al_2O_3	AC conductivity 150–400 °C	3×10^{-11} * 5×10^{-8} *	0.88 0.57	35

4. Conclusion

The Li-ion conductivity in amorphous LiAlO₂ films deposited by atomic layer deposition (ALD) has been investigated on films deposited on insulating sapphire and conducting Ti substrates by impedance spectroscopy using, respectively, in-plane and cross-plane geometries. The conductivity in these films exhibit ionic conduction, presumably by Li ions, with Arrhenius-type activated temperature dependency. The room-temperature conductivity of LiAlO₂ films is in the range of $\sim 10^{-10}$ Scm⁻¹, and the activation energy is *ca.* 0.8 eV. In-plane and cross-plane methods have been compared: In-plane conductivities exhibit stronger thickness-dependence especially with thin film thickness (90 nm here), which can be tentatively attributed to effects of the large interface and surface of that geometry. Better reproducibility is achieved using the cross-plane geometry showing close conductivity values in 90, 160 and 235 nm films, once short-circuit from film damage as a result of fabrication or handling can be avoided.

Acknowledgments

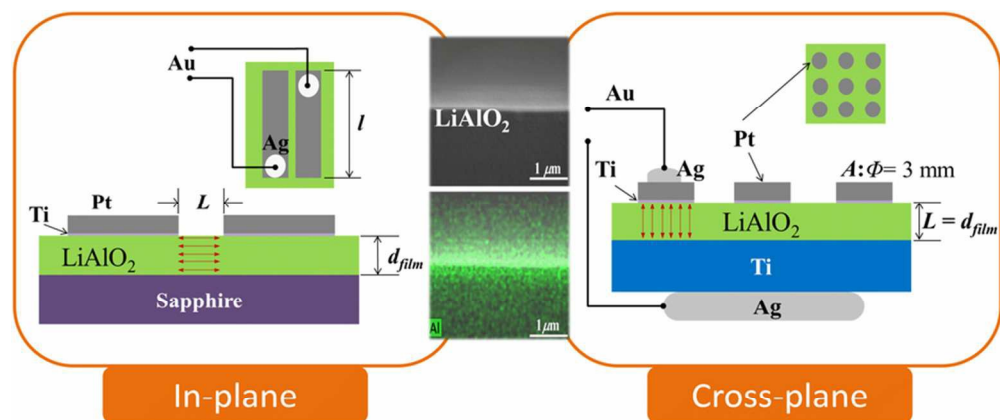
The authors thank Drs. A. Evans and S. Kumar (University of Oslo, UiO) for fruitful discussions and V. Bobal (UiO MiNaLab) for technical assistance. The financial support by the Research Council of Norway via projects 220135 NanoMILiB and 200030 3DBatt is gratefully acknowledged, as well as the Norwegian Micro- and Nano-Fabrication Facility, NorFab (197411/V30).

References

- 1 J. F. M. Oudenhoven, L. Baggetto and P. H. L. Notten, *Adv Energy Mater*, 2011, **1**, 10-33.
- 2 J. L. Souquet and M. Duclot, *Solid State Ionics*, 2002, **148**, 375-379.
- 3 N. J. Dudney, *Mat Sci Eng B-Solid*, 2005, **116**, 245-249.
- 4 K. Takada, *Acta Mater.*, 2013, **61**, 759-770.

- 5 M. Park, X. Zhang, M. Chung, G. B. Less and A. M. Sastry, *J. Power Sources*, 2010, **195**, 7904-7929.
- 6 S.-J. Lee, H.-K. Baik and S.-M. Lee, *Electrochem. Commun.*, 2003, **5**, 32-35.
- 7 M. Roberts, P. Johns, J. Owen, D. Brandell, K. Edstrom, G. El Enany, C. Guery, D. Golodnitsky, M. Lacey, C. Lecoecur, H. Mazor, E. Peled, E. Perre, M. M. Shaijumon, P. Simon and P.-L. Taberna, *J. Mater. Chem.*, 2011, **21**, 9876-9890.
- 8 J. W. Long, B. Dunn, D. R. Rolison and H. S. White, *Chemical Reviews*, 2004, **104**, 4463-4492.
- 9 M. Putkonen, T. Aaltonen, M. Alnes, T. Sajavaara, O. Nilsen and H. Fjellvåg, *J. Mater. Chem.*, 2009, **19**, 8767-8771.
- 10 R. L. Puurunen, *J. Appl. Phys.*, 2005, **97**, 121301.
- 11 T. Aaltonen, O. Nilsen, A. Magrasó and H. Fjellvåg, *Chem. Mater.*, 2011, **23**, 4669-4675.
- 12 J. Liu, M. N. Banis, X. Li, A. Lushington, M. Cai, R. Li, T.-K. Sham and X. Sun, *J. Phys. Chem. C*, 2013, DOI: 10.1021/jp4063302, 20260-20267.
- 13 I. D. Scott, Y. S. Jung, A. S. Cavanagh, Y. Yan, A. C. Dillon, S. M. George and S.-H. Lee, *Nano Lett.*, 2010, **11**, 414-418.
- 14 M. E. Donders, H. C. Knoops, W. M. M. Kessels and P. H. Notten, *ECS Transactions*, 2011, **41**, 321-330.
- 15 E. Østreg, K. B. Gandrud, Y. Hu, O. Nilsen and H. Fjellvåg, *J. Mater. Chem. A*, 2014, **2**, 15044-15051.
- 16 V. Miikkulainen, O. Nilsen, M. Laitinen, T. Sajavaara and H. Fjellvåg, *RSC Advances*, 2013, **3**, 7537-7542.
- 17 J. S. Park, X. Meng, J. W. Elam, S. Hao, C. Wolverton, C. Kim and J. Cabana, *Chemistry of Materials*, 2014, **26**, 3128-3134.
- 18 A. C. Kozen, A. J. Pearse, C.-F. Lin, M. Noked and G. W. Rubloff, *Chem. Mater.*, 2015, **27**, 5324-5331.
- 19 X. Yu, J. B. Bates, G. E. Jellison and F. X. Hart, *J. Electrochem. Soc.*, 1997, **144**, 524-532.
- 20 D. J. Kalita, S. H. Lee, K. S. Lee, D. H. Ko and Y. S. Yoon, *Solid State Ionics*, 2012, **229**, 14-19.
- 21 K.-H. Joo, H.-J. Sohn, P. Vinatier, B. Pecquenard and A. Levasseur, *Electrochem. Solid-State Lett.*, 2004, **7**, A256-A258.
- 22 S. Sanna, V. Esposito, J. W. Andreasen, J. Hjelm, W. Zhang, T. Kasama, S. B. Simonsen, M. Christensen, S. Linderoth and N. Pryds, *Nat Mater*, 2015, **14**, 500-504.
- 23 E. Navickas, M. Gerstl, G. Friedbacher, F. Kubel and J. Fleig, *Solid State Ionics*, 2012, **211**, 58-64.
- 24 D. J. Comstock and J. W. Elam, *The Journal of Physical Chemistry C*, 2012, **117**, 1677-1683.
- 25 V. Thangadurai and W. Weppner, *Adv. Funct. Mater.*, 2005, **15**, 107-112.
- 26 K. Benaissa, P. V. Ashrit, G. Bader, F. E. Girouard and V.-V. Truong, *Thin Solid Films*, 1992, **214**, 219-222.

- 27 V. Thangadurai, R. A. Huggins and W. Weppner, *J. Power Sources*, 2002, **108**, 64-69.
- 28 M. Gerstl, E. Navickas, G. Friedbacher, F. Kubel, M. Ahrens and J. Fleig, *Solid State Ionics*, 2011, **185**, 32-41.
- 29 C. Li, L. Gu and J. Maier, *Adv. Funct. Mater.*, 2012, **22**, 1145-1149.
- 30 S. Ross, A.-M. Welsch and H. Behrens, *PCCP*, 2015, **17**, 465-474.
- 31 S.-i. Furusawa, A. Kamiyama and T. Tsurui, *Solid State Ionics*, 2008, **179**, 536-542.
- 32 J. Li, N. J. Dudney, J. Nanda and C. Liang, *ACS Applied Materials & Interfaces*, 2014, **6**, 10083-10088.
- 33 S. Indris, P. Heitjans, R. Uecker and B. Roling, *J. Phys. Chem. C*, 2012, **116**, 14243-14247.
- 34 S. Konishi and H. Ohno, *J. Am. Ceram. Soc.*, 1984, **67**, 418-419.
- 35 A. M. Glass and K. Nassau, *J. Appl. Phys.*, 1980, **51**, 3756-3761.
- 36 J. Fu, *Solid State Ionics*, 1997, **104**, 191-194.



Comparison of in-plane and cross-plane conductivity on ALD-deposited LiAlO_2 thin films

80x39mm (300 x 300 DPI)